Available online at www.sciencedirect.com
ScienceDirect
Ceramics International 37 (2011) 3477–3487
CERAMICS INTERNATIONAL
www.elsevier.com/locate/ceramint

Synthesis of carbon-free Si_3N_4/SiC nanopowders using silica fume

Jyothi Suri [a], Leon L. Shaw [a,*], Mahmoud F. Zawrah [b]

[a] Department of Chemical, Materials and Biomolecular Engineering University of Connecticut, Storrs, CT 06269, USA
[b] Ceramics Department, National Research Center, 12622 Dokki, Cairo, Egypt

Received 16 March 2011; received in revised form 28 May 2011; accepted 6 June 2011
Available online 12 June 2011

Abstract

We have investigated a possible method of synthesizing carbon-free, nano-silicon nitride–silicon carbide (Si_3N_4/SiC) powders from the waste silica fume for the first time, using the integrated mechanical and thermal activation (IMTA) process. This novel process results in the formation of nano-Si_3N_4/SiC powders at 1465 °C with crystallite sizes as small as 45 nm. In order to synthesize carbon-free nano-Si_3N_4/SiC powders, two different approaches, one using the H_2 gas and the other using air, have been studied for their effectiveness in removing the free carbon present. It is found that the H_2 treatment is not very effective although both Si_3N_4 and SiC are stable during the H_2 treatment. In contrast, removing the free carbon using air is effective, and the limited oxidation of nano-Si_3N_4 and SiC can be achieved if the air treatment is terminated soon after the free carbon is eliminated. This study has provided a clear pathway and understanding for effectively synthesizing carbon-free, nano-Si_3N_4/SiC powders from the silica fume.

Keywords: Silicon nitride; Silicon carbide; Nanocrystalline ceramics; Carbothermic reduction and nitridation

1. Introduction

Silica fume containing 94–97 wt% of silicon dioxide (SiO_2) is the waste material produced from silicon metal and ferro-silicon alloy industry. It is formed during the reduction of pure quartz (SiO_2) by carbon, in the presence of iron, on heating in electric furnaces up to ≥1750 °C, hence its name silica fume. A portion of the gas formed during this reduction process escapes through the furnace charge with waste gases, which is oxidized in air, cooled and separated as microsilica dust by electrostatic filters or filter-bags. This fume has to be collected to prevent it from polluting the environment. Owing to the fine particle size, high SiO_2 content and large surface area of the fume, it can be used as a pozzolan to improve the properties of concrete [1]. Furthermore, silica fume has been found to improve the compressive strength, bond strength, and abrasion resistance of concrete, and reduce the permeability and thus help in protecting steel from corrosion [1–3].

Silicon nitride–silicon carbide (Si_3N_4/SiC) nanocomposites have potential for high temperature structural applications, such as turbine and automobile engine components and heat exchangers, as well as energy applications due to their good mechanical and thermal properties at both room and elevated temperatures [4–7]. A number of approaches to achieve these composite powders include chemical vapor decomposition of Si–C–N precursors [8–10], pyrolysis of liquid organic precursors [11], thermal decomposition of methane on sub-micron Si_3N_4 powders and physical mixture of sub-micron Si_3N_4 and SiC commercial powders [12,13], each having their own advantages and disadvantages. Synthesis of pure Si_3N_4 and SiC powders has also been studied extensively in the last three decades. For example, carbothermic reduction of silica has been studied to synthesize pure SiC powder [14,15], whereas carbothermic reduction and nitridation of silica has been investigated to form pure Si_3N_4 powder [16–18]. Other methods such as vapor-phase reactions [19,20] have also been pursued and resulted in the formation of Si_3N_4 and SiC at very low temperatures (i.e., 650 and 1100 °C, respectively).

The present study focuses on the synthesis of carbon-free Si_3N_4/SiC nano-powders using silica fume and graphite as the starting raw materials. Furthermore, substantial efforts of this study have been devoted to investigating an effective way to remove the excess carbon present in the nano-Si_3N_4/SiC powder synthesized in this study. The processing approach of

* Corresponding author.
E-mail address: leon.shaw@uconn.edu (L.L. Shaw).

0272-8842/$36.00
doi:10.1016/j.ceramint.2011.06.003

this study to convert the waste silica fume to advanced Si_3N_4/SiC nanocomposites is based on a process called as the integrated mechanical and thermal activation (IMTA) process, developed recently for synthesizing large quantities of low cost, high quality, nanostructured carbides and nitrides [7,21–24]. The mechanical activation of the reactants at room temperature by high-energy ball milling increases the reactivity of the reactants and dramatically reduces the temperature and time of the synthesis reaction. However, as will be shown later, the nano-Si_3N_4/SiC powder synthesized from the IMTA process contains excess carbon (termed as the free carbon in this study because it does not form compounds with other elements). Uncontrolled amounts of free carbon are detrimental to the sintering of Si_3N_4 and SiC powders either through liquid phase sintering with oxide sintering aids [25–28] or through solid state sintering with a small amount of C and B [29,30]. Thus, two types of treatments have been investigated in order to eliminate the free carbon in the as-synthesized nano-Si_3N_4/SiC powder. One treatment uses the H_2 gas to remove the free carbon, while the other uses the air atmosphere. Although both of these treatments have been studied before to remove the free carbon present in SiC and Si_3N_4 powders separately [31–35], the present study has resulted in the additional understanding and offers a direct comparison of the effectiveness between the two treatments. As will be shown later, substantial differences are present between these two treatments. Therefore, a comparative study is essential especially when a large amount of the free carbon is present. Through this study a clear pathway and understanding for effectively synthesizing carbon-free, nano-Si_3N_4/SiC powders from the silica fume have been established.

2. Experimental

The raw materials to synthesize Si_3N_4/SiC nanocomposite powders are the silica fume acquired from Egyptian Company for Ferro-Alloys (Edfu, Aswan, Egypt), and the graphite powder of 99.5% purity (-100 mesh) from Alfa Aesar (Ward Hill, MA, USA). The as-received graphite powder was high-energy ball milled at room temperature for 6 h and then mixed with the silica fume in the graphite-to-silica fume molar ratio of 6:1. The milling was carried out in a modified Szegvari attritor from Union Process Inc., which was shown to be effective in synthesizing a uniform milling product within the powder charge [36]. The charge consisted of WC balls of 4.76 mm in diameter and $SiO_2 + C$ powders at a ball-to-powder ratio of 60:1. The charged canister was evacuated up to 10^{-3} Torr, flushed with high purity argon (99.95%), followed by evacuation and finally filled with argon at a pressure of about 1.5 atm. Milling was carried out in the argon atmosphere at a speed of 600 rpm for 6 h. The milling canister was made of stainless steel and cooled with circulation water (20 °C) at a flow rate of 770 ml/min throughout the entire process. The temperature of canister was monitored using an E-type thermocouple attached to the bottom of canister.

The ball milled mixture ($SiO_2 + C$) in the form of loose powder was subjected to carbothermal reduction and nitridation reactions. A known amount of the ball milled mixture ($SiO_2 + C$) was placed in an alumina crucible which was then inserted into the furnace. The carbothermal reduction and nitridation was conducted in a ceramic tube furnace which was evacuated up to 7×10^{-4} Torr ($\sim 9 \times 10^{-2}$ Pa) before the onset of heating. This was followed by backfilling with the ultra high purity nitrogen gas (procured from Airgas Company) at a flow rate of ~ 2 m^3/h for 60 min before the onset of reaction. The average heating rate was 8 °C/min and the samples were heated to 1465 °C and held at that temperature for 2 h before cooling to room temperature. The flow of nitrogen is maintained at the rate of ~ 2 m^3/h during the entire heating, holding and cooling processes. The nano-powders obtained following the carbothermal reduction and nitridation were found to contain free carbon (a detailed description follows in Section 3), in addition to the Si_3N_4 and SiC phases. Since excess free carbon is detrimental to the sintering of nano-Si_3N_4/SiC powders, elimination of free carbon from these nano-powders is necessary. Free carbon elimination was studied under two different atmospheres: hydrogen and air. The carbon elimination was carried out in a tube furnace with a flowing atmosphere (either H_2 or air) at a rate of 1 m^3/h. The reaction temperature and duration were variables and studied in order to obtain carbon-free, nano-Si_3N_4/SiC powders. Details of these experimental conditions will be discussed along with results.

In order to identify the reaction pathway and monitor the completion of reactions during free carbon removal processes, the effluent gas from the tube furnace was constantly monitored using a quadrupole residual gas analyzer (RGA) equipped with a mass spectrometer (Model ppt-c300-F2Y). By monitoring the intensity change of the gaseous species in the outlet gas from the reaction furnace using a RGA, one can detect the presence of gaseous species and how they change as a function of temperature and reaction time, thereby deducing the reaction pathway(s). The gaseous species monitored by the RGA included H_2, N_2, O_2, H_2O, CO_2, CO, CH_4, SiO and Ar. This was achieved by monitoring the species with a mass-to-charge ratio of 2 (corresponding to H_2^+), 16 (CH_4^+ and O^+), 18 (H_2O^+), 28 (N_2^+ and CO^+), 32 (O_2^+), 40 (Ar^+), and 44 (SiO^+ and CO_2^+).

To unambiguously provide the evidence of removing the free carbon and to quantify the amount of the free carbon removed in carbon elimination experiments, pure graphite ball milled for 6 h was also subjected to carbon elimination experiments. Studies of this type avoided the interference of the potential reaction of nano-Si_3N_4 and SiC with the carbon removing gas, and thus offered a clear guideline for judicial selection of the carbon elimination condition. The weights of the powders before and after the carbon elimination treatment were measured to compute the percentage of the free carbon eliminated in the carbon elimination process.

The chemical analysis of the as-received silica fume was carried out using X-ray florescence (XRF) based on wavelength dispersive spectrometry (Axios, Panalytical 2005). The morphology and sizes of the as-milled and reacted powders were examined using a field emission scanning electron microscope (FESEM, JEOL 6335) operated at 10 kV. Individual phases were analyzed using X-ray diffraction

(XRD) with CuK$_\alpha$ radiation, 40 kV, 40 mA, 1°/min, and 0.02° per step using a D5005 ADVANCE diffractometer. The average crystallite size was estimated using the Scherrer formula without the consideration of internal strains [37,38],

$$D = \frac{0.9\,\lambda}{B_g(2\theta)\cos\theta} \quad (1)$$

where $B_g(2\theta)$ is the broadening of the diffraction line measured at half maximum intensity, λ is the wave length of the X-ray radiation, and θ is the Bragg angle. In addition to phase identification, the XRD analysis was also utilized to estimate the relative quantities of Si_3N_4 and SiC in the final powder mixture. The multiline mean-normalized-intensity method [39,40] was adopted for this purpose. In this method, the volume fraction of the i phase, v_i, in the sample can be evaluated via Eq. (2)

$$\upsilon_i = \frac{\bar{I}_i^n}{\sum_p \bar{I}_p^n} \quad (2)$$

where $\bar{I}_i^n$ is the mean normalized intensity of the i phase and $\sum_p \bar{I}_p^n$ is the summation over all p phases in the sample. The mean normalized intensity of the i phase in the sample can be obtained by averaging the normalized intensities of the selected Bragg peaks of the i phase. The normalized intensity of Bragg peak j of the i phase, I_{ij}^n, can be calculated with the aid of Eq. (3) [39]

$$I_{ij}^n = \frac{I_{ij}}{R_{ij}} \quad (3)$$

where I_{ij} is the integrated intensity of Bragg peak j of the i phase and R_{ij} is the normalizing factor for Bragg peak j of the i phase. In the present study the R_{ij} values for α-Si_3N_4 were taken from Ref. [40], while the R_{ij} values for α-SiC (4H polytype) were computed in this study.

The presence of the free carbon in the nano-Si_3N_4/SiC powder under various conditions was studied using Raman spectroscopy. Raman spectra were obtained using a dispersive spectrometer Renishaw Ramascope - 2000 containing an argon-ion laser, Leica DMLM microscope. The laser was operated at 514 nm and its power at the sample was 50 mW, with a neutral density filter of 25% and a spectral resolution of about 1 cm^{-1}. The objective at 50× magnification was used to collect scattered light from spots as small as 1.0 μm in diameter. The spectra were obtained with exposure time of 160 s per scan from multiple locations on the sample, and analyzed using WIRE2 software.

3. Results and discussion

3.1. Characterization of the starting materials

The as-received silica fume (Fig. 1a) are spherical particles with a diameter ranging from ~10 nm to less than 500 nm, with majorities of particles around 100 nm. Fig. 1b shows the XRD pattern of the silica fume, revealing that it is amorphous because there are no crystalline peaks except a weak and broad

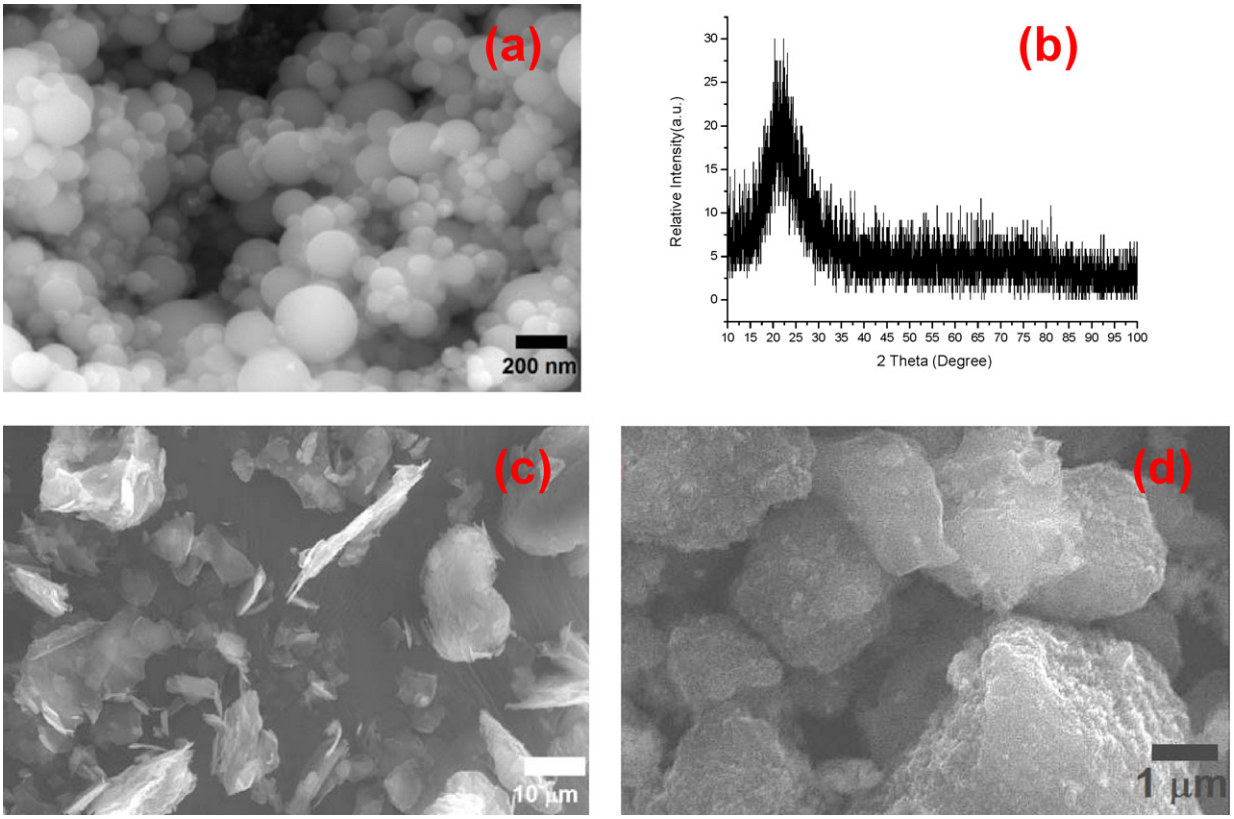

Fig. 1. (a) An SEM image of the as-received silica fume, (b) its XRD pattern, (c) and (d) SEM images of graphite before and after ball milling alone for 6 h, respectively.

Table 1
Chemical composition of the as-received silica fume.

Oxide	SiO_2	Al_2O_3	Fe_2O_3	CaO	MgO	Na_2O	K_2O	LOI[a]	SO_3
wt.%	94.53	0.79	2.22	0.48	1.12	0.03	0.02	1.25	0.10

[a] LOI stands for loss of ignition.

peak near 21°. Table 1 summarizes the chemical analysis of the silica fume, revealing that it contains 94 wt.% of SiO_2 with major impurities of Fe_2O_3 (2.22 wt.%) and MgO (1.12 wt.%). Fig. 1c and d shows the SEM images of graphite before and after ball milling, respectively. Before ball milling, graphite has flake morphology with a dimension of approximately 1 μm × 10 μm × 10 μm. After 6-h of ball milling, graphite particles have become round and their average sizes have been reduced to 1–5 μm in diameter. This enables uniform mixing of the silica fume with the ball milled graphite.

Fig. 2a shows the SEM image of the SiO_2 + C mixture after ball milling for 6 h, and Fig. 2b presents the corresponding XRD pattern. It can be seen from the XRD pattern that the silica fume remains to be amorphous after ball milling. Crystalline graphite, however, has become nanoscale or near amorphous as evidenced by a broad peak at ~26.4° (JCPDS 41-1487). The presence of WC peaks (JCPDS 25-1047) is due to the wear debris of WC/Co balls used in ball milling. The quantity of these impurities, however, is low. Based on the wear rate of 5.5 mg/h determined previously under similar ball milling conditions [41], the weight percent of WC/Co in the powder mixture milled for 6 h is estimated to be ~0.15 wt.%. In spite of the low concentration, the WC peaks are quite strong because of the high mass absorption coefficient of WC for the X-ray radiation in comparison with graphite [38]. Also, trace amounts of Co are observed, from the wear debris of WC/Co balls. No detectable XRD peaks of Fe were observed in the as-milled mixtures, and thus contamination from the stainless steel canister, if any, is lower than the detection limit of the XRD analysis.

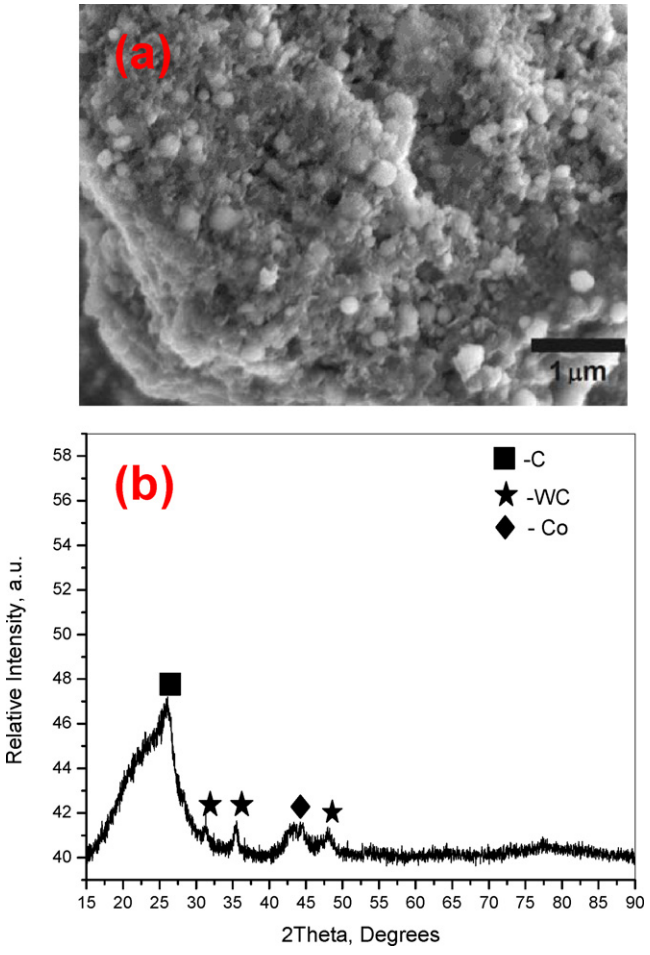

Fig. 2. (a) The SEM image of the SiO_2 + C mixture after ball milling for 6 h, showing the sizes and morphology of the primary particles that form agglomerates, and (b) its XRD pattern.

A comparison among Figs. 1a, c and d and 2a reveals that the bead morphology of the silica fume has more or less survived the ball milling process, but graphite particles have been refined. Moreover, agglomeration has taken place during ball milling, and the silica fume and graphite have mixed uniformly within agglomerates. The size of agglomerates ranges from less than 10 μm to about 30 μm (not shown here), and each agglomerate contains hundreds of fine silica fume and graphite particles most of which have sizes between 10 and 500 nm (Fig. 2a). Thus, the particle refinement and uniform mixing have been accomplished through high-energy ball milling and will facilitate the formation of nanostructured Si_3N_4/SiC powder through the subsequent carbothermic reduction and nitridation reaction.

3.2. Synthesis of nano-Si_3N_4/SiC powders

The powder mixture after ball milling for 6 h was subsequently subjected to the carbothermic reduction and nitridation reaction at 1465 °C for 2 h in a nitrogen atmosphere. The XRD pattern of the reaction product (Fig. 3a) shows the formation of α-Si_3N_4 (JCPDS 41-0360) and α-SiC (JCPDS 29-1127, a 4H polytype SiC), with the presence of a trace amount of β-Si_3N_4 (JCPDS 40-1129) and some unreacted graphite (JCPDS 41-1487). The latter with a broad peak at 26.4° is clearly inherited from the powder mixture before the carbothermic reduction and nitridation (see Fig. 2b). The unreacted graphite is due to the excess graphite added in the starting powder in order to completely convert the silica fume to Si_3N_4 and SiC and to increase the Si_3N_4 content in the reaction product. It is well known that graphite particles provide the sites for nucleation of Si_3N_4 crystals, and thus the more graphite, the more Si_3N_4 nuclei and more Si_3N_4 content in the reaction product [31]. The amounts of Si_3N_4 and SiC formed in the

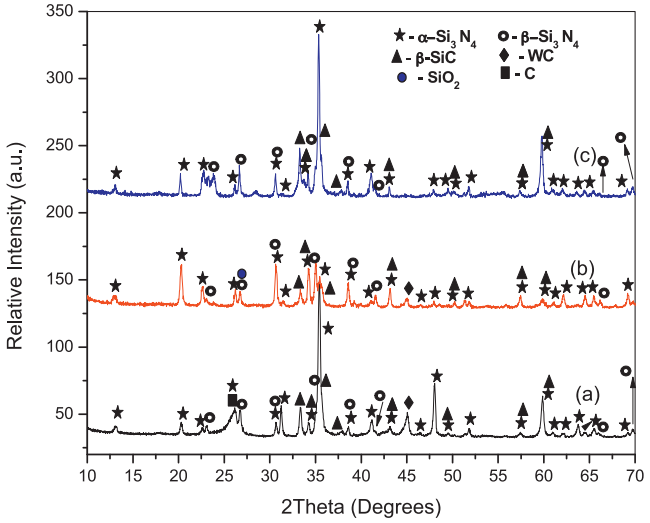

Fig. 3. XRD patterns of the silica fume plus graphite mixture: (a) subjected to carbothermic reduction and nitridation at 1465 °C in a nitrogen atmosphere for 2 h, (b) after carbon elimination at 700 °C in air for 2 h, and (c) after the SiO_2-removal treatment with HF acid at the ambient environment for 4 h.

reaction product have been estimated using the multiline mean-normalized-intensity method [39,40]. Only the relative quantities of α-Si_3N_4 and α-SiC have been included in this estimation because the quantities of β-Si_3N_4 and WC contaminant are small. The mean normalized intensity of α-Si_3N_4 is computed based on the α-Si_3N_4 (1 0 1), (1 1 0), (2 0 0) and (2 0 1) peaks, while the corresponding value of α-SiC is obtained from the α-SiC (1 0 0), (1 0 2) and (0 0 4) peaks. Through this method the volume fractions of α-Si_3N_4 and α-SiC in the reaction product are estimated to be 66 and 34%, respectively.

The SEM images of the as-synthesized Si_3N_4/SiC powder are shown in Fig. 4a and b, which reveal that Si_3N_4 and SiC have both particle and whisker morphologies. The whisker nature of these powders arises due to a number of factors such as the flowing atmosphere during the carbothermic reaction, annealing condition during carbothermic condition, milling time, etc. [24]. The powder is agglomerated and the sizes of the primary particles forming these agglomerates are from 80 to 500 nm. However, the crystallite sizes of Si_3N_4 and SiC particles estimated from XRD using the Scherrer formula are 45 and 58 nm, respectively. A comparison between the primary particle sizes observed using SEM and the crystallite sizes estimated from XRD suggests that the primary particles forming agglomerates are polycrystals and thus each primary particle has multiple nuclei for the growth of Si_3N_4 and SiC grains during carbothermic reduction and nitridation.

These results demonstrate that nano-Si_3N_4/SiC powder can be produced from waste silica fume. Furthermore, ~66 vol.% Si_3N_4 formed at 1465 °C obtained in this study is relatively

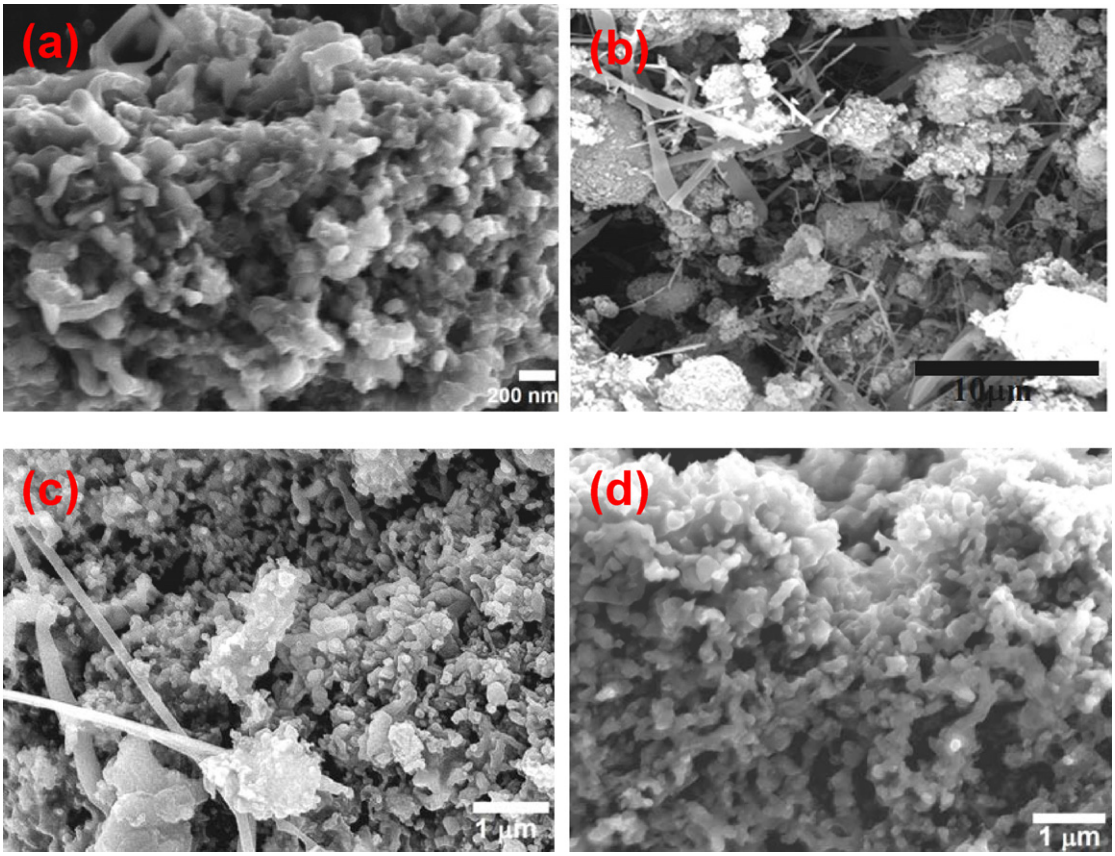

Fig. 4. SEM images of the nano-Si_3N_4/SiC powders: (a) and (b) the as-synthesized powder showing both particle and whisker morphologies and the formation of agglomerates, (c) after carbon elimination at 700 °C in air for 2 h, and (d) after the SiO_2-removal treatment with HF acid at the ambient environment for 4 h.

high. Previous studies [17,18] require 1500 to 1550 °C to achieve high Si_3N_4 contents. In addition, the formation of SiC at 1465 °C is one of the lowest temperatures through carbothermic reduction to form SiC reported in the open literature [15,41,42]. The enhanced formation of Si_3N_4 and SiC in this study is attributed to the mechanical activation induced by high-energy ball milling before carbothermic reduction and nitridation, while the nanocrystalline nature of the Si_3N_4/SiC powder is ascribed to the low synthesis temperature and the fine particle sizes induced by high-energy ball milling before the synthesis.

3.3. Elimination of free carbon from the as-synthesized nano-Si_3N_4 and SiC powders

In this study a high graphite concentration is used to convert the entire silica fume to nano-Si_3N_4/SiC and to attain a high Si_3N_4 concentration in the final product. However, using a high graphite concentration results in the presence of a large amount of the free carbon in the as-synthesized nano-Si_3N_4/SiC powder. Therefore, the as-synthesized nano-Si_3N_4/SiC powder has been studied for removal of the free carbon under two different atmospheres, hydrogen and air. It should be emphasized that hydrogen treatments have been studied before to remove free carbon in SiC fibers and powders, and proven to be adequate when the amount of free carbon is low [32–35]. However, when the quantity of free carbon is high, hydrogen treatments may not be very effective [32], which is confirmed by the present study. For this reason, air treatments are also investigated in this study in order to provide an effective method to eliminate the free carbon in the as-synthesized nano-Si_3N_4/SiC powder.

Since there are three major phases (i.e., Si_3N_4, SiC and C) in the as-synthesized nano-Si_3N_4/SiC powder, all of the possible reactions of these three phases with hydrogen and air have to be considered in order to have a good control of the treatment. For this purpose, the thermodynamic calculations of the possible reactions have been performed based on the data compiled by Knacke et al. [43] with the assumption that every gas involved has a pressure of 0.1 MPa. Table 2 lists all the possible reactions with hydrogen, while Table 3 summarizes all the possible reactions with the oxygen in air. Fig. 5 shows the free energy of reaction as a function of temperature for all of the reactions that have a favorable thermodynamic driving force. Note that both Si_3N_4 and SiC are stable under the H_2 atmosphere in the temperature range of interest (Table 2). The only thermodynamically favorable reactions are C with H_2 (i.e., reaction H6) and SiC with H_2 in the presence of H_2O (reaction H7). Since there is no H_2O steam in the present study, reaction H7 is not possible. In contrast, reaction H6 is possible because the continuous H_2 flow during the experiment can maintain the H_2 pressure at 0.1 MPa while taking away the reaction product, CH_4, continuously. Thus, the H_2 treatment has the advantage of removing the free carbon while both Si_3N_4 and SiC are stable. However, as shown in Fig. 5a, the driving force for reaction H6 is quite small (achieved through continuously removing CH_4 from the tube furnace by flowing H_2 continuously). For this reason, the H_2 treatment temperature in this study has been selected at 700 °C (973 K) with a flowing H_2 atmosphere in order to have sufficient reaction kinetics and at the same time remove CH_4 from the furnace.

Fig. 6a shows the compositional profile of the effluent gas from the tube furnace, acquired using the RGA, for the H_2

Table 2
Thermodynamic data of Si_3N_4, SiC and C under the H_2 atmosphere in the temperature range 800–1300 K[a] [43].

Reaction no.	Reaction	Temperature range (K)	Gibbs Free Energy (kJ/mol)
H1	$Si_3N_4 + 12H_2 = 3SiH_4 + 4NH_3$	800–1000	Positive
H2	$Si_3N_4 + 2H_2 = 3SiH_4 + 2N_2$	800–1000	Positive
H3	$Si_3N_4 + H_2 = 3Si + 2N_2 + H_2$	800–1300	Positive
H4	$SiC + 4H_2 = SiH_4 + CH_4$	800–1000	Positive
H5	$SiC + 2H_2 = Si + CH_4$	800–1300	Positive
H6	$C + 2H_2 = CH_4$	800–1300	Negative–positive
H7	$SiC + H_2O + H_2 = 0.5Si + 0.5SiO_2 + CH_4$	800–1300	Negative

[a] Some reactions have only been considered in the temperature range from 800 to 1000 K because of the lack of the thermodynamic data.

Table 3
Thermodynamic data of Si_3N_4, SiC and C under the oxygen atmosphere in the temperature range 800–1300 K [43].

Reaction no.	Reaction	Temperature range (K)	Free energy (kJ/mol)
O1	$Si_3N_4 + 3O_2 = 3SiO_2 + 2N_2$	800–1300	Negative
O2	$Si_3N_4 + 5O_2 = 3SiO_2 + 4NO$	800–1300	Negative
O3	$SiC + 2O_2 = SiO_2 + CO_2$	800–1300	Negative
O4	$SiC + 1.5O_2 = SiO_2 + CO$	800–1300	Negative
O5	$SiC + O_2 = SiO + CO$	800–1300	Negative
O6	$C + 0.5O_2 = CO$	800–1300	Negative
O7	$C + O_2 = CO_2$	800–1300	Negative

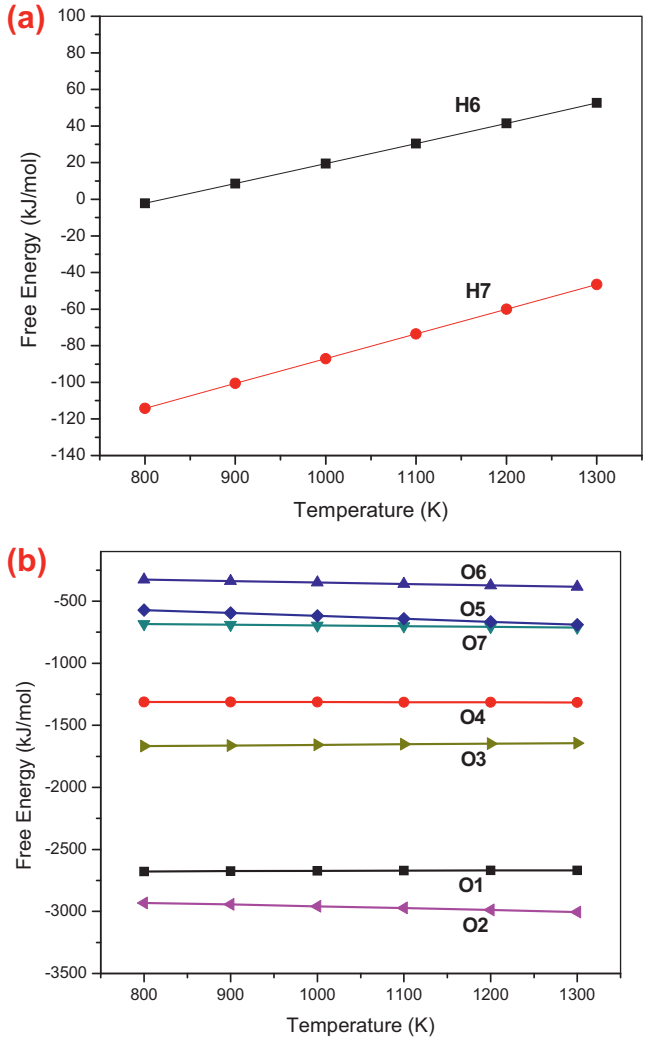

Fig. 5. The Gibbs free energies of reactions as a function of temperature: (a) under a hydrogen atmosphere and (b) under an oxygen atmosphere. The specific reactions indicated can be found in Tables 2 and 3.

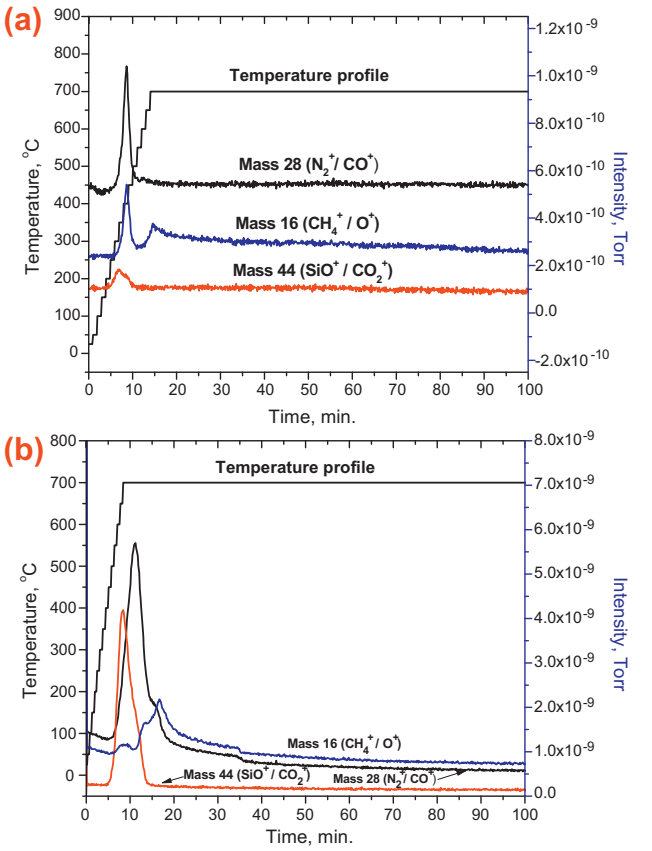

Fig. 6. The composition profile of the effluent gas during the H2 treatment at 700 °C for 8 h: (a) the as-synthesized nano-Si_3N_4/SiC powder and (b) the pure graphite ball milled alone for 6 h.

treatment at 700 °C for 8 h. The heating stage is also included in figure, but for the clarity, only the compositional profile in the first 100 min is shown because there is no peak in the remaining 380-min holding. Note that only the intensities of the species with the mass-to-charge ratio of 16 (CH_4^+ and O^+), 28 (N_2^+ and CO^+) and 44 (SiO^+ and CO_2^+), termed hereafter as Mass 16, Mass 28 and Mass 44 respectively, are shown in this figure because other species do not provide direct information about the nature of the carbon elimination treatment. It can be seen that the intensities of Mass 16, 28 and 44 increase substantially during heating between 180 and 500 °C. The peak of Mass 28 is attributed to the generation of CO mainly by reaction O6 (in Table 3), which takes place because the free carbon in the as-synthesized nano-Si_3N_4/SiC powder reacts with the residual oxygen present in the tube furnace before flowing the H_2 gas. This reaction is confirmed by the H_2 treatment of pure graphite (to be discussed later). Similarly, the peak of Mass 44 is ascribed to the generation of CO_2 mainly by reaction O7, which is also supported by the H_2 treatment of pure graphite to be shown later. Note that reactions O3–O5 can produce CO and CO_2, while reaction O1 can generate N_2. However, all of these reactions proceed very slowly because the formation of solid SiO_2 or SiO on the surfaces of SiC and Si_3N_4 particles can drastically prevent the further oxidation of the remaining SiC and Si_3N_4 cores [44,45].

The peaks of Mass 16 are attributed to the generation of CH_4 through reaction H6 in Table 2. The presence of two peaks is presumably related to the size distribution of the free carbon particles although more detailed studies are needed to confirm this. Note that the intensity of the second peak decreases gradually as the holding time increases, and the gradual decrease of this peak continues even after holding for 8 h (not shown here), suggesting that the removal of the free carbon via reaction H6 to form CH_4 (Table 2) is very ineffective and there is still free carbon in the powder after the H_2 gas treatment at 700 °C for 8 h. The weight loss of the powder before and after the carbon elimination treatment at 700 °C for 8 h is found to be 30%.

In order to simplify the analysis of removing the free carbon in the carbon elimination experiment, pure graphite ball milled for 6 h is also subjected to the H_2 treatment. Fig. 6b shows the intensities of Mass 16, 28 and 44 as a function of the treatment time and temperature for this treatment. The overall profiles of Mass 16, 28 and 44 for the pure graphite are similar to those for

the as-synthesized nano-Si_3N_4/SiC powder (Fig. 6a), i.e., most of the graphite has reacted with the hydrogen gas and the residual oxygen during heating as well as at the early stage of holding. The similarity between Fig. 6a and b confirms that Mass 28 and 44 are indeed predominantly due to reactions O6 and O7, respectively. However, different behaviors are present between these two sets of experiments with two being particularly notable. One is the much higher intensities of Mass 16, 28 and 44 for the pure graphite sample than that for the as-synthesized nano-Si_3N_4/SiC powder. This trend has been attributed to the 100% carbon in the pure graphite sample versus a small amount of the free carbon in the as-synthesized nano-Si_3N_4/SiC powder. The other difference is the shifting of various peaks to higher temperatures when the sample changes from the as-synthesized nano-Si_3N_4/SiC powder to the pure graphite. We suggest that this shifting is due to the larger particle sizes in the pure graphite sample than that in the as-synthesized nano-Si_3N_4/SiC powder. The graphite in the as-synthesized nano-Si_3N_4/SiC powder is finer (Fig. 2 versus Fig. 1) because it has been ball milled for a total of 12 h (i.e., 6 h in the form of pure graphite plus another 6 h with the silica fume). At the end of the 8-h treatment for the pure graphite experiment, some graphite is still present and the weight loss is found to be only 36%, confirming that hydrogen treatment at 700 °C is not effective in removing all graphite. This result is consistent with the thermodynamic calculation (Table 2 and Fig. 5a), showing that the driving force for reaction H6 is very small.

To enhance the elimination of the free carbon in the as-synthesized nano-Si_3N_4/SiC powder, carbon elimination has been changed to oxidation of the as-synthesized nano-Si_3N_4/SiC powder under air. As shown in Table 3 and Fig. 5b, all the species in the nano-powder, i.e., Si_3N_4, SiC and C, have favorable thermodynamic driving forces to react with oxygen. Thus, the key to the success of the air treatment is to maximize the reaction between the free carbon and oxygen while minimizing the reaction of Si_3N_4 and SiC with oxygen. Compressed air is used in this study to enable the controlled flow of air. The holding temperature is 700 °C, the same as that employed in the H_2 treatment. The temperature and compositional profiles of the oxidation treatment are shown in Fig. 7. Only Mass 44 is shown in these figures because Mass 16 (CH_4^+) is irrelevant in the oxidation treatment and Mass 28 (N_2^+ and CO^+) is dominated by the N_2^+ species in air. Note that the intensity of Mass 44 (SiO^+ and CO_2^+) in Fig. 7 is an order of magnitude higher than that shown in Fig. 6, suggesting that with sufficient oxygen supply the reaction between the free carbon and oxygen can be quite intensive. The weight loss of the sample before and after the carbon elimination treatment is found to be 40%. This has resulted in complete elimination of the free carbon from the as-synthesized nano-Si_3N_4/SiC powder, as will be discussed later.

In order to confirm that the strong intensity of Mass 44 is indeed predominately due to the reaction between the free carbon and oxygen (reaction O7) rather than reaction O5 to form SiO (Table 3), pure graphite ball milled for 6 h is also subjected to the air treatment at 700 °C for 2 h. Fig. 7b shows

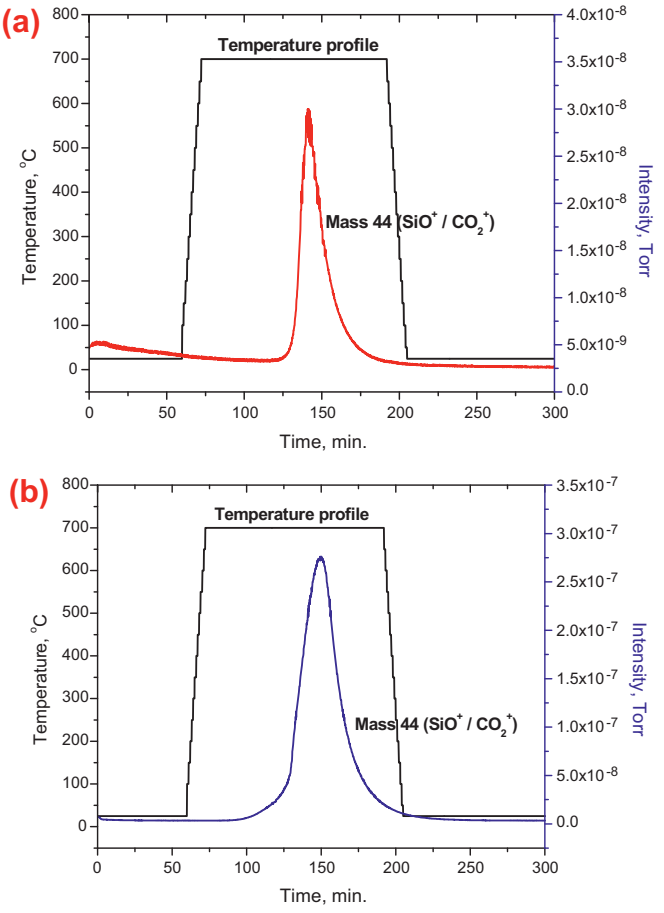

Fig. 7. The composition profile of the effluent gas during the air treatment at 700 °C for 2 h: (a) the as-synthesized nano-Si_3N_4/SiC powder and (b) the pure graphite ball milled alone for 6 h.

the composition profile of Mass 44 for this experiment. The similar peak positions of Mass 44 as a function of the holding time in Fig. 7a and b strongly suggest that this peak is mainly due to reaction O7. The fact that the intensity of Mass 44 for the pure graphite sample is one order of magnitude higher than that for the as-synthesized nano-Si_3N_4/SiC also supports that the notion that the peak of Mass 44 in Fig. 7a is dominated by the reaction between the free carbon and oxygen rather than reaction O5. The total weight loss of the pure graphite sample before and after the carbon elimination treatment is found to be 93%. This result is consistent with the RGA analysis (Fig. 7b), which shows that at the end of the 2-h holding a small amount of CO_2 is still being generated, indicating that a small amount of graphite is still present inside the furnace. However, this is not the case for the as-synthesized nano-Si_3N_4/SiC powder. As shown in Fig. 7a, at the end of the 2-h holding the intensity of Mass 44 has dropped to the background level corresponding to the CO_2 present in air. The fact that the free carbon in the as-synthesized nano-Si_3N_4/SiC powder reacts with oxygen faster than the pure graphite ball milled for 6 h is due to the finer particle size of the free carbon in the as-synthesized nano-Si_3N_4/SiC powder. Based on the RGA data, it can then be concluded that all of the free carbon in the as-synthesized nano-

Si_3N_4/SiC powder has been removed via the air treatment at 700 °C for 2 h. This conclusion is confirmed by Raman spectroscopy as detailed later. Since additional oxidation treatment beyond 2 h can lead to excessive oxidation of nano-Si_3N_4 and SiC, 700 °C for 2 h under a flowing air atmosphere has been chosen as the final condition to remove the free carbon in the as-synthesized nano-Si_3N_4/SiC powder.

Finally, it should be pointed out that although reactions O1–O4 have much larger thermodynamic driving forces than reactions O6 and O7, reactions O1–O4 can only proceed with a very slow rate. This is due to the formation of SiO_2 from reactions O1 to O4. The SiO_2 product on the surface of SiC and Si_3N_4 can drastically reduce the oxidation of the remaining SiC and Si_3N_4 cores because diffusion of oxygen through the solid SiO_2 shell is required for further oxidation [44,45]. In contrast, the products of reactions O6 and O7 are gases. As a result, graphite is always exposed to oxygen and oxidation can proceed with a linear rate if a flowing oxygen atmosphere is maintained [46]. Reaction O5 produces a solid SiO shell on the surfaces of SiC particles. Thus, like reactions O1–O4, reaction O5 proceeds very slowly because the continuation of reaction O5 requires diffusion of oxygen through the solid SiO shell.

3.4. Characterization of carbon-free, nano-Si_3N_4/SiC powders

Fig. 3b shows the XRD pattern of the as-synthesized nano-Si_3N_4/SiC after the free-carbon removal treatment at 700 °C in air for 2 h. It can be seen that the unsymmetric peak at 26.4° due to the free carbon in the as-synthesized nano-Si_3N_4/SiC (Fig. 3a) has been eliminated via the air treatment. However, several interesting phenomena have occurred along with the elimination of the free carbon. First, the most noticeable change is the dramatic reduction in the intensity of α-Si_3N_4 (2 1 0) peak at 35.51°. This reduction is attributed to the oxidation of Si_3N_4 during the air treatment, leading to the formation of a thin layer of SiO_2 on the surfaces of Si_3N_4 particles. Many of other peaks such as (0 0 2) at 31.85°, (2 1 2) at 48.06°, and (3 1 2) and (3 2 0) at 59.84° also exhibit substantial decreases in their intensities, owing to the coverage of a thin layer of SiO_2 on the surfaces of Si_3N_4 particles.

Second, it is surprising to note that the relative intensities of some Si_3N_4 peaks, e.g., (1 0 1) at 20.61°, (2 0 1) at 31.02°, and (2 1 1) at 38.93°, have increased with respect to other Si_3N_4 peaks. We propose that this phenomenon is due to the uneven oxidation rates on different surfaces made of different crystallographic planes of Si_3N_4 crystals. As a result, the reduction in the sizes of Si_3N_4 crystals depends on the crystallographic direction and the thickness of the SiO_2 layer formed on the surfaces of Si_3N_4 crystals also varies with the crystallographic direction. These uneven reductions in the sizes of Si_3N_4 crystals and different thicknesses of SiO_2 layers lead to substantial reduction in the intensity for some peaks with small reduction for other peaks.

Third, another unexpected phenomenon has been noted, that is, the intensity of the Si_3N_4 (2 0 0) peak at 26.54° has decreased. This peak overlaps with the strongest peak of SiO_2, the (1 0 1) peak at 26.67° (JCPDS 33-1161). One would expect the intensity of this peak to increase because of the oxidation of Si_3N_4 and the overlap of the two peaks. We suggest that the unexpected behavior is due to the substantial oxidation of Si_3N_4 on the surface made of the (2 0 0) planes. As a result, the intensity of the Si_3N_4 (2 0 0) peak has reduced dramatically because of the coverage of SiO_2 layer on that surface of Si_3N_4 crystals, and the peak at 26.54° in Fig. 3b has a significant contribution from SiO_2. This viewpoint is corroborated by the fourth phenomenon mentioned below.

Fourth, it is noted that the relative intensities of all Si_3N4 peaks except (0 0 2) at 31.85° and (2 1 2) at 48.06° recover after the SiO_2-removal treatment with HF acid (Fig. 3c). This supports the hypothesis of the coverage of SiO_2 on the surfaces of Si_3N_4 crystals discussed above. The non-recovery of (0 0 2) and (2 1 2) peaks may suggest that the surfaces of Si_3N_4 crystals made of (0 0 2) and (2 1 2) crystallographic planes suffer more oxidation than the surfaces made of other crystallographic planes.

Fifth, uneven peak intensity changes have also occurred to SiC crystals. For example, the SiC (1 0 0) peak at 33.35° has decreased its relative intensity, while the SiC (1 0 1) peak at 34.78° has increased its relative intensity along with the Si_3N_4 (1 0 2) peak after the air treatment at 700 °C. Both of these peaks, however, recover their relative intensities after the subsequent SiO_2-removal treatment with HF acid. Similar to Si_3N_4 crystals, the uneven peak intensity changes can again be interpreted as the result of different oxidation rates on different surfaces of SiC crystals.

Finally, it should be emphasized that the uneven intensity changes are not due to errors during XRD data collection because every sample shown in Fig. 3 has been subjected to three separate XRD analyses. The XRD patterns from these three independent experiments show excellent repeatability. Therefore, the uneven intensity changes are due to the changes in the powder mixtures after different treatments as discussed above. Thus, based on the RGA and XRD analyses we can conclude that the air treatment can remove the free carbon in the as-synthesized nano-Si_3N_4/SiC powder while avoiding the substantial oxidation of nano-Si_3N_4 and SiC particles. Furthermore, the HF treatment is effective in eliminating SiO_2 introduced during the air treatment.

Since XRD is not sensitive to the presence of a small amount of carbon, Raman spectroscopy has been utilized to study the change of the free carbon in the nano-Si_3N_4/SiC powder at various stages. Fig. 8 shows the Raman bands at ~1355 cm^{-1} (D band), ~1580 cm^{-1} (G band) and ~1620 cm^{-1} (D′ band) of graphite at various conditions. The G band is Raman active for sp^2 carbon networks, while the D and D′ bands are used to investigate the formation of defects [47,48]. It is noted that the as-received graphite powder has a much sharper G band than the ball milled counterparts. Furthermore, the D and D′ band widths increase substantially as the ball milling time increases (Fig. 8a–c), indicating the introduction of a large amount of defects into graphite by ball milling [49]. Fig. 8d–h shows the Raman spectra obtained from nano-Si_3N_4/SiC powders after the carbon removal treatment under different conditions. These

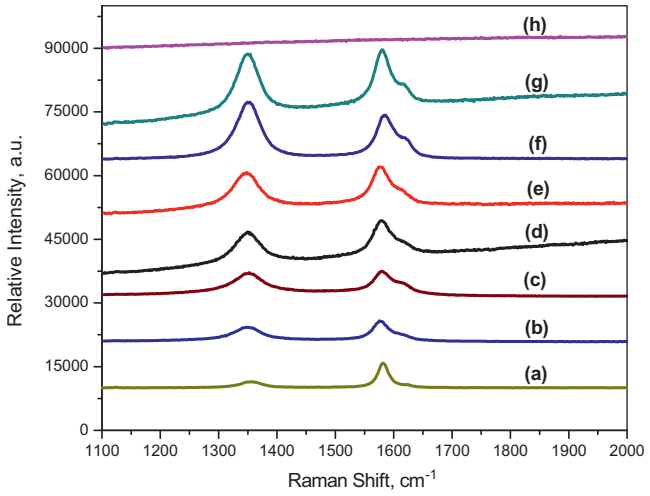

Fig. 8. Raman spectra obtained from: (a) the as-received graphite powder, (b) the graphite powder ball milled alone for 6 h, and (c) the 6 h ball milled graphite mixed with the silica fume and ball milled for another 6 h. Other spectra are related to the nano-Si_3N_4/SiC powder after subjecting to various carbon elimination treatments: (d) 700 °C in H_2 for 8 h, (e) 800 °C in H_2 for 8 h, (f) 900 °C in H_2 for 7 h, (g) 1000 °C in H_2 for 7 h, and (h) 700 °C in air for 2 h.

spectra clearly reveal that the H_2 treatment under various conditions at temperatures ranging from 700 to 1000 °C (spectra d–g) is not effective in removing the free carbon in the as-synthesized nano-Si_3N_4/SiC because of the presence of the D, G and D′ bands in the spectra. In contrast, the air treatment at 700 °C for 2 h is very effective in completely eliminating the free carbon (spectrum h). These results are in excellent agreement with the RGA analyses shown in Figs. 6 and 7 and consistent with the thermodynamic calculations summarized in Fig. 5 and Tables 2 and 3.

The SEM images of nano-Si_3N_4/SiC powders after the air treatment and then after the HF treatments are shown in Fig. 4c and d, respectively. It can be seen that there is no obvious change in the size of the primary particles forming the agglomerates before and after various treatments. However, the agglomerates after treatments are more porous than the counterparts before any treatment. These results indicate that the air treatment and the subsequent HF treatment do not affect Si_3N_4 and SiC particle sizes much, but can effectively remove the free carbon and then SiO_2 so that Si_3N_4/SiC agglomerates become porous.

4. Conclusions

The present study demonstrates that nano-Si_3N_4/SiC composite powders can be synthesized using the silica fume, a low cost silica source. The crystallite sizes of Si_3N_4 and SiC are as small as 45 nm, and their particle sizes range from 80 to 500 nm. These primary particles form agglomerates with sizes from 10 to 30 μm. The carbothermic reduction and nitridation reaction carried out at 1465 °C resulted in the synthesis of ~66 vol.% Si_3N_4 + 34 vol.% SiC powders. The investigation of removing the free carbon in the as-synthesized nano-Si_3N_4/SiC reveals that the H_2 treatment is not very effective although both Si_3N_4 and SiC are stable during the H_2 treatment. In contrast, removing the free carbon using air is effective, and the limited oxidation of nano-Si_3N_4 and SiC can be achieved if the air treatment is terminated soon after the free carbon is eliminated. The extent of carbon elimination is not only dictated by thermodynamic driving forces, but also by the reaction kinetics, that is, it depends on reaction duration, the particle size, and the quantity of the free carbon present before the carbon elimination treatment. Thus, this study has provided a clear pathway and understanding for effectively synthesizing carbon-free, nano-Si_3N_4/SiC powders from silica fume.

Acknowledgements

The authors, J.S. and L.S., would like to thank the U.S. National Science Foundation (NSF) and U.S.–Egypt Joint Science & Technology Board for the financial support under the grant number OISE-0913886. The author, M.Z., is indebted to the Science and Technology Development Fund (STDF), Ministry of Scientific Research, Egypt for the financial support under the U.S.–Egypt joint program (Project ID 858).

References

[1] ACI Committee 226, Silica fume in concrete: preliminary report, ACI Mater. J. 84 (1987) 158–166.
[2] M. Pigeon, P. Plante, M. Plante, Air-void stability. Part I: influence of silica fume and other parameters, ACI Mater. J. 86 (1989) 482–490.
[3] J. Wolsiefer, Ultra high-strength field placeable concrete with silica fume admixture, Concr. Int. Des. Constr. 6 (1984) 25–31.
[4] K. Niihara, New design concept of structural ceramics. Ceramic nanocomposites, J. Ceram. Soc. Jpn. Int. Ed. 99 (1991) 945–952.
[5] K. Niihara, A. Nakahira, T. Sekino, Y.-H. Choa, Development of ceramic based nanocomposites with high performance, J. Jpn. Soc. Powder Metall. 44 (1997) 887–896.
[6] G. Pezzotti, Si_3N_4–SiC-platelet composite without sintering aids: a candidate for gas turbine engines, J. Am. Ceram. Soc. 76 (1993) 1313–1320.
[7] L.L. Shaw, Z.G. Yang, R.M. Ren, Synthesis of nanostructured Si_3N_4/SiC composite powders through high energy reaction milling, Mater. Sci. Eng. A 244 (1998) 113–126.
[8] K. Niihara, K. Izaki, T. Kawakami, Hot-pressed Si_3N_4-32% SiC nanocomposite from amorphous Si–C–N powder with improved strength above 1200C, J. Mater. Sci. Lett. 10 (1991) 112–114.
[9] K. Niihara, K. Izaki, A. Nakahira, Nano-composite materials based on Si_3N_4 and SiC, Adv. Ceram. 56–57 (1991) 319–326.
[10] K. Niihara, K. Suganuma, A. Nakahira, K. Izaki, Interfaces in Si_3N_4–SiC nano-composite, J. Mater. Sci. Lett. 9 (1990) 598–599.
[11] G. Ziegler, J. Hapke, Synthesis and pyrolysis of liquid organometallic precursors for advanced Si–Ti–C–N composites, Adv. Mater. 7 (1995) 380–384.
[12] K. Watari, K. Ishizaki, M. Kawamoto, Behavior of carbon in hot pressed silicon nitride grain boundaries and its influence on mechanical properties, Yogyo-Kyokai-Shi 96 (1988) 127–133.
[13] J. Tian, J. Li, L. Dong, Synthesis of silicon nitride/silicon carbide nanocomposite powders through partial reduction of silicon nitride by pyrolyzed carbon, J. Am. Ceram. Soc. 82 (1999) 2548–2550.
[14] V.M. Kevorkijan, M. Koman, D. Kolar, Low-temperature synthesis of sinterable SiC powders by carbothermic reduction of colloidal SiO_2, J. Mater. Sci. 27 (1992) 2705–2712.

[15] R. Koc, S.V. Cattamanchi, Synthesis of beta silicon carbide powders using carbon coated fumed silica, J. Mater. Sci. 33 (1998) 2537–2549.
[16] T. Licko, V. Figusch, J. Puchyova, Synthesis of silicon nitride by carbothermal reduction and nitriding of silica: control of kinetics and morphology, J. Eur. Ceram. Soc. 9 (1992) 219–230.
[17] S.J.P. Durham, K. Shanker, R.A.L. Drew, Carbothermal synthesis of silicon nitride: effect of reaction conditions, J. Am. Ceram. Soc. 74 (1991) 31–37.
[18] M. Ekelund, B. Forslund, Carbothermal preparation of silicon nitride: influence of starting material and synthesis parameters, J. Am. Ceram. Soc. 75 (1992) 532–539.
[19] S. Kavecky, B. Janekova, J. Madejova, P. Sajgalik, Silicon carbide powder synthesis by chemical vapour deposition from silane/acetylene reaction system, J. Eur. Ceram. Soc. 20 (2000) 1939–1946.
[20] S. Sahu, S. Kavecky, J. Szepvolgyi, Preparation of fine amorphous silicon nitride powder in the system SiH_4–Ar–NH_3, J. Eur. Ceram. Soc. 15 (1995) 1071–1077.
[21] R. Ren, Z. Yang, L.L. Shaw, Novel process for synthesizing nanostructured carbides: mechanically activated synthesis, Ceram. Eng. Sci. Proc. 19 (1998) 461–468.
[22] R. Ren, Z. Yang, L.L. Shaw, Synthesis of nanostructured silicon carbide through an integrated mechanical and thermal activation process, J. Am. Ceram. Soc. 85 (2002) 819–827.
[23] L.L. Shaw, Processing of nanostructured carbides, nitrides, and their composites, Adv. Eng. Mater. 2 (2000) 721–723.
[24] L.L. Shaw, Z. Yang, R. Ren, Dependence of silicon carbide product morphology on the degree of mechanical activation, J. Am. Ceram. Soc. 85 (2002) 709–711.
[25] D.F. Carroll, A.W. Weimer, S.D. Dunmead, G.A. Eisman, J.H. Hwang, G.A. Cochran, D.W. Susnitzky, D.R. Beaman, C.L. Conner, Carbothermally prepared nanophase SiC/Si_3N_4 composite powders and densified parts, AIChE J. 43 (1997) 2624–2635.
[26] J. Grabis, D. Jankovica, M. Berzins, L. Chera, Preparation of silicon carbide/nitride particulate nanocomposites with oxides or nitrides, Diffus. Defect Data Pt. B 94 (2003) 151–156.
[27] M. Herrmann, C. Schuber, A. Rendtel, H. Hübner, Silicon nitride/silicon carbide nanocomposite materials: I. Fabrication and mechanical properties at room temperature, J. Am. Ceram. Soc. 81 (1998) 1095–1108.
[28] M. Hnatko, D. Galusek, P. Sajgalik, Low-cost preparation of Si_3N_4–SiC micro/nano composites by in-situ carbothermal reduction of silica in silicon nitride matrix, J. Eur. Ceram. Soc. 24 (2004) 189–195.
[29] G.H. Wroblewska, E. Nold, F. Thummler, The role of boron and carbon additions on the microstructural development of pressureless sintered silicon carbide, Ceram. Int. 16 (1990) 201–209.
[30] S. Prochazka, R.M. Scanlan, Effect of boron and carbon on sintering of SiC, J. Am. Ceram. Soc. 58 (1975) 72.
[31] S.C. Zhang, W.R. Cannon, Preparation of silicon nitride from silica, J. Am. Ceram. Soc. 67 (1984) 691–695.
[32] Y. Zhong, L.L. Shaw, M. Manjarres, M.F. Zawrah, Synthesis of silicon carbide nanopowder using silica fume, J. Am. Ceram. Soc. 93 (2010) 3159–3167.
[33] T. Shimoo, Y. Katase, K. Okamura, W. Takano, Carbon elimination by heat-treatment in hydrogen and its effect on thermal stability of polycarbosilane-derived silicon carbide fibers, J. Mater. Sci. 39 (2004) 6243–6251.
[34] A.T. Hemida, R. Pailler, R. Naslain, Continuous SiC-based model monofilaments with a low free carbon content, part I: from the pyrolysis of a polycarbosilane precursor under an atmosphere of hydrogen, J. Mater. Sci. 32 (1997) 2359–2366.
[35] A.T. Hemida, R. Pailler, R. Naslain, J.P. Pillot, M. Birot, J. Dunogues, Continuous SiC-based model monofilaments with a low free carbon content, part II: from the pyrolysis of a novel copolymer precursor, J. Mater. Sci. 32 (1997) 2367–2372.
[36] Z.G. Yang, L.L. Shaw, Synthesis of nanocrystalline SiC at ambient temperature through high energy reaction milling, Nanostruct. Mater. 7 (1996) 873–886.
[37] W.H. Hall, X-ray line broadening in metals, Proc. Phys. Soc. A 62 (1949) 741–747.
[38] H.P. Klung, X-ray Diffraction Procedures for Polycrystalline and Amorphous Materials, John Wiley & Sons Inc., London, 1954.
[39] D.Y. Li, B.H. O'Connor, Q.T. Chen, M.G. Zadnik, Quantitative powder X-ray diffractometry phase analysis of silicon nitride materials by a multiline mean-normalized-intensity method, J. Am. Ceram. Soc. 77 (1994) 2195–2198.
[40] J.P. Nicolich, Z. Lences, W. Dressler, R. Riedel, Phase quantification of β-Si_3N_4/β-SiC mixtures by X-ray powder diffraction analysis, J. Mater. Sci. 35 (2000) 1427–1432.
[41] Z. Yang, R. Ren, X. Xie, L.L. Shaw, On nitrogen sorption during high energy milling of silicon powders in ammonia and nitrogen, Metall. Mater. Trans. A 30 (1999) 1109–1117.
[42] R.V. Krishna Rao, M.M. Godkhindi, R.G.I. Mukunda, M. Chakraborty, Direct pyrolysis of rice husks for maximization of silicon carbide whisker formation, J. Am. Ceram. Soc. 74 (1991) 2869–2875.
[43] O. Knacke, O. Kubaschewski, K. Hesselmann, Thermo-chemical Properties of Inorganic Substances, second ed., Springer-Verlag, Berlin, 1991.
[44] J. Quanli, Z. Haijun, L. Suping, J. Xiaolin, Effect of particle size on oxidation of silicon carbide powders, Ceram. Int. 33 (2007) 309–313.
[45] S.C. Singhal, Thermodynamics and kinetics of oxidation of hot-pressed silicon nitride, J. Mater. Sci. 11 (1976) 500–509.
[46] L. Shaw, W. Osborn, T. Markmaitree, X. Wan, The reaction pathway and rate-limiting step of dehydrogenation of $LiHN_2$ + LiH mixture, J. Power Sources 177 (2008) 500–505.
[47] A.C. Ferrari, J.C. Meyer, V. Scardaci, C. Casiraghi, M. Lazzeri, F. Mauri, S. Piscanec, D. Jiang, K.S. Novoselov, S. Roth, A.K. Geim, Raman spectrum of graphene and graphene layers, Phys. Rev. Lett. 97 (2006), 187401-1-4.
[48] A. Gupta, G. Chen, P. Joshi, S. Tadigadapa, P.C. Eklund, Raman scattering from high-frequency phonons in supported n-graphene layer films, Nano Lett. 6 (2006) 2667–2673.
[49] Z.G. Huang, Z.P. Guo, A. Calka, D. Wexler, J. Wu, P.H.L. Notten, H.K. Liu, Noticeable improvement in the desorption temperature from graphite in rehydrogenated MgH_2/graphite composite, Mater. Sci. Eng. A 447 (2007) 180–185.